Quasipatterns in a polarization instability

D. Leduc, M. Le Berre, E. Ressayre, and A. Tallet
Laboratoire de Photophysique Moléculaire du CNRS, Bâtiment 213, Université Paris–Sud, 91405 Orsay Cedex, France
(Received 23 June 1995)

The nonlinear analysis of the model equation for the single-feedback-mirror device with rubidium atoms predicts that a stable quasipattern of eightfold orientational order occurs in the profile of the output light beam. This pattern is numerically reproduced for different transverse shapes, either rhombohedric or circular, of the input beam.

PACS number(s): 42.65.−k, 42.55.−f

I. INTRODUCTION

Spatial patterns, such as rolls, squares, and hexagons, discovered in hydrodynamics [1], also occur in nonlinear optics [2]. The first experiment that displayed such patterns was realized with a distributed-feedback system with a passive sodium vapor [3]. The same typical patterns have also been recently reported in the case of a polarization instability with a rubidium vapor cell [4,5].

Quasiperiodic patterns, or ''quasipatterns,'' with eightfold [6] or 12-fold orientational order [7,8] have recently been observed in Faraday instability [7] and theoretically discussed with the help of a Swift-Hohenberg-type equation for a real amplitude [9]. Two different models have been considered for explaining these quasipatterns. The first one assumes that the amplitude is a superposition of single set of N (>3) modes $\mathbf{K}_i$ with the same length K; but this assumption requires a complex nonlinearity involving high powers of the transverse Laplacian ∇_t^2, in order to generate the coupling between the N modes. Such a nonlinear interaction seems unlikely in hydrodynamics, so that the single-wave-number model was left for explaining the quasipatterns in the Faraday instability. The other model assumes two sets of N modes, with two different wave numbers K and q, related via a triadic interaction. This latter model appears to describe qualitatively well the physics related to the experiment of Edwards and Fauve [7], in which the instability is driven by a two-frequency force, inducing a quadratic coupling.

Differently from hydrodynamics, optics can easily provide model equations involving high powers of the transverse Laplacian ∇_t^2, more precisely the exponential operator $\exp[i\nabla_t^2(z/2k)]$ diffracting a light beam with longitudinal wave number k, that propagates along a distance z, along its optical axis. Devices such as the single-feedback mirror device [5,10,11], the unidirectional passive ring cavity [12], or the liquid-crystal light valve loop device [13] carry out the interplay between nonlinearities and the free-space diffraction that operates on the complex amplitude of the electric field emerging from a nonlinear cell. With this latter device, quasipatterns of eightfold, tenfold, etc., eighteenfold orientational order have been observed, but the four, five, etc., nine modes associated with these patterns are those predicted to occur with the help of the linear stability analysis, as a result of the rotation imposed to the feedback [14,15].

In this paper, the quasipatterns that are analytically predicted and numerically obtained are the signature of a nonlinear regime. The system under study is the single-feedback-mirror optical arrangement with a rubidium vapor cell, which has displayed sequences of flowerlike patterns [10] in the limit of small aspect ratios [16]. Here we treat the limiting case of large aspect ratios and we show that this device is a good candidate for the observation of quasipatterns, associated with a single set of four, six, etc., modes, as discussed by Müller [9] in his first model. This system obeys, indeed the two following requirements: (a) it provides a cubic nonlinearity and (b) it may support the coexistence of more than two or three modes.

The paper is organized as follows. In Sec. II the Bloch and Maxwell equations for the device [5,11] are shown to reduce to a single partial differential equation for the nonlinear refractive index $Q(t,x,y)$ inside the cell. It is shown that the D_1 line of rubidium provides a polarization instability through a cubic nonlinearity. The plane-wave linear stability analysis predicts a degenerate multiconical emission on both sides of resonance [16]: The two infinite sets of critical wave numbers K_j are given by

$$\frac{d}{k}K_j^2=\frac{\pi}{2}(1+4j) \tag{1a}$$

on the focusing side and

$$\frac{d}{k}K_j^2=\frac{\pi}{2}(3+4j) \tag{1b}$$

on the defocusing side.

In practice, input beams have a finite width, which leads to the removal of the degeneracy of the multiconical emission. Therefore, near threshold, only the largest critical wavelength is involved in the building of the transverse structure of the output light beam. The introduction of a diffusionlike process also contributes to favor the onset of the instability on the cone associated with the smallest critical wave number. Otherwise, it is possible to choose another critical wave number by introducing some filter in the far field in order to suppress the undesirable part(s) of the spectrum.

The amplitude equations are derived by assuming that the transverse structure is built with the help of a single set of N modes with the same wave number. The Landau coefficient that couples two modes $\mathbf{K}$ and $\mathbf{K}'$, such as $\phi=(\mathbf{K},\mathbf{K}')$, is shown to obey the relation

$$\beta(\phi)=1-\cos\left(\frac{2d}{k}K^2\cos\phi\right), \tag{2}$$

with $K=|\mathbf{K}|$. This coupling coefficient is always positive when ϕ varies from 0 to π, whatever K might be, and presents one or several zeros, depending on the magnitude of K. The number of the minima M of the Landau coefficient defines the number of modes that may coexist with the mode $\mathbf{K}$. Then, if each of the $M+1$ modes can coexist with the others, a far-field pattern made of $2(M+1)$ spots lying on a circle of radius K is expected: On the focusing side, with the smallest critical wave number K_1, $\beta(\phi)$ displays a single minimum for $\phi=\pi/2$, predicting the coexistence of two orthogonal modes, leading to the occurrence of squares. On the defocusing side, still with the smallest wave number as given by Eq. (1b), $\beta(\phi)$ displays three minima, predicting that a mode $\mathbf{K}_i$ can coexist with other three modes $\mathbf{K}_j$: Therefore a pattern built with the help of four modes is expected, giving rise in the far field to eight spots lying on a circle of radius K_1. In Sec. IV the numerical results obtained near threshold are presented. They agree with the predictions of the nonlinear analysis and eightfold orientational order quasipatterns are shown. This structure is obtained for any transverse shape of the input beam that is either a circular or a rhombic window. The single feedback device with a Rb gaseous cell, under study, is, to our knowledge, the first physical (at least optical) system in which an eightfold orientational order quasipattern is predicted to occur, due to nonlinearities.

For larger critical wave numbers, the number of minima of the Landau coefficient increases so that the system might generate quasipatterns of 12-fold orientational order on the focusing side and 16-fold orientational order on the defocusing side, still with a single set of wave vectors. Unfortunately, these structures are shown to be unstable.

II. MODEL

The atomic cell of length l is illuminated by a continuous, homogeneous, and linearly polarized laser beam with angular frequency ω, real amplitude ε_x, and transverse width w_0. This laser beam propagates in the forward direction and is in resonance with the D_1 line of the rubidium ^{85}Rb. The Rb transition $5S_{1/2}(F=3)\rightarrow 5P_{1/2}(F'=2)$ is simplified as a $J=\frac{1}{2}\rightarrow J=\frac{1}{2}$ transition. The upper sublevels $|e;\pm\frac{1}{2}\rangle$ and the lower states $|g;\mp\frac{1}{2}\rangle$ are coupled via the circularly polarized field components of the electromagnetic field σ^+ and σ^-. The usual adiabatic approximation applies for this transition, because the radiative lifetime of the excited levels Γ^{-1} is much smaller than the mean time of the interaction of an atom with the electromagnetic field γ^{-1}: Typically, this time is equal to the width of the input beam divided by the thermal mean velocity $\langle u\rangle$, i.e.,

$$\gamma=\frac{\langle u\rangle}{2w_0}\ll\Gamma. \tag{3}$$

Furthermore, for input intensity $\mathcal{I}_0$ much smaller than the off-resonance saturation intensity $3\mathcal{I}_S$

$$\frac{\mathcal{I}_0}{3\mathcal{I}_S}\ll 1, \tag{4}$$

the population of the excited states is negligible. [$\mathcal{I}_S=(6\hbar^2/\mu^2)\Gamma^2(1+\Delta^2)$, where μ and $\Delta=(2/\Gamma)(\omega-\omega_a)$ are the dipolar momentum and the detuning scaled to $\Gamma/2$, respectively]. The situation, where the populations of the upper states are not negligible, was treated by Hamilton, Ballagh, and Sandle [17].

Finally, when the two above inequalities (3) and (4) are fulfilled, the Bloch equations for a Rb atom, located at z in the cell, reduce to a single differential equation for the population difference of the Zeeman lower sublevels [18,19] $J_3(z,t)$,

$$\frac{\partial J_3}{\partial t}=-2\gamma[(1+I_++I_-)J_3+(I_+-I_-)], \tag{5}$$

where $I_\pm$ are the intensities [see Eq. (5)] associated with the crossed circular polarizations $\sigma_\pm$, respectively, scaled to the ''saturation'' intensity associated with the lower Zeeman sublevels $(3\Gamma/2\gamma)\mathcal{I}_S$, i.e., $I_\pm=\mathcal{I}_\pm(2\gamma/3\Gamma\mathcal{I}_S)$. They are

$$I_\pm=|\varepsilon_f^\pm e^{ikz}+\varepsilon_b^\pm e^{-ikz}|^2, \tag{6}$$

where $\varepsilon_{f,b}$ are the forward and backward field amplitudes, respectively. The amplitude field components obey the following reduced Maxwell equations, where α is the off-resonance absorption length:

$$\frac{\partial\varepsilon_f^\pm}{\partial z}=-\frac{\alpha(1+i\Delta)}{2}\varepsilon_f^\pm[1\pm J_3], \tag{7a}$$

$$\frac{\partial\varepsilon_b^\pm}{\partial z}=+\frac{\alpha(1+i\Delta)}{2}\varepsilon_b^\pm[1\pm J_3]. \tag{7b}$$

In the reduced Maxwell equations (7), the coupling between the forward and backward field amplitudes is neglected because the mean lifetime of the grating, displayed by the crossed term of Eq. (6), γ^{-1}, is much larger than the mean time $\pi/k\langle u\rangle$ spent by an atom propagating along a grating length. [Indeed, when using Eq. (3), the inequality $\gamma^{-1}\gg(k\langle u\rangle)^{-1}$ becomes $kw_0\gg 1$, which is satisfied for the atomic transition under study.] It follows that the intensities $I_\pm$, defined in Eq. (6), reduce to the sum of the forward and backward intensities. The diffraction inside the cell is also neglected because the conditions

$$l\ll d\ll Z_d, \tag{8}$$

which are fulfilled in the experiment of Grynberg, Maitre, and Petrossian [11], are assumed in the model [4,5] (Z_d is the Rayleigh length $\frac{1}{2}kw_0^2$).

The boundary conditions are

$$\varepsilon_f^\pm(z=0,t,\mathbf{r})=\frac{1}{\sqrt{2}}\varepsilon_x(\mathbf{r}), \tag{9a}$$

$$\varepsilon_b^\pm(z=l,t,\mathbf{r})=R\exp\left(i\frac{d\nabla_t^2}{k}\right)\varepsilon_f^\pm(z=l,t,\mathbf{r}). \tag{9b}$$

Equation (9b) expresses the free-space propagation of the output forward field amplitude, after is has been reflected by a plane mirror with reflectivity R, located at the distance d of

the cell exit. (The time delay is neglected because it is much smaller than any characteristic time of the system.)

The stationary solution of $J_3(z)$, see Eq. (5), is proportional to the source term $(I^+ - I^-)$ and then vanishes for electric fields with a linear polarization, as assumed in Eq. (9a). The onset of an instability removes the degeneracy of the Zeeman sublevels and generates an electromagnetic field component with the crossed linear polarization $\vec{e}_y$, making the source term $(I_+ - I_-)$ different from zero.

The integration over the propagation variable z of the coupled equations (5) and (7) can be analytically performed [16], leading to a single differential equation for the quantity $\int_0^l dz\ J_3(z)$. But in the limit of no pump depletion $\alpha l \ll 1$, a simpler expression arises: The integration of Eq. (7a) gives rise to

$$\varepsilon_f^{\pm}(z=l,t,\mathbf{r}) = \frac{1}{\sqrt{2}}\,\varepsilon_x(\mathbf{r}) \exp\left[\frac{-i\alpha l\Delta}{2}\,(1 \pm J_3)\right] \quad (10a)$$

or, in the limit of a plane-wave input, with $\varepsilon_x(\mathbf{r}) = \varepsilon_0$,

$$\varepsilon_f^{\pm}(z=l,t,\mathbf{r}) = \frac{1}{\sqrt{2}}\,\varepsilon_0 \exp\left[\frac{-i\alpha l\Delta}{2}\,(1 \pm J_3)\right], \quad (10b)$$

so that Eq. (9b) becomes

$$\varepsilon_b^{\pm}(z=l,t,\mathbf{r}) = \frac{1}{\sqrt{2}}\,R\varepsilon_0 \exp\left(i\,\frac{d\nabla_t^2}{k}\right)\exp\left[\frac{-i\alpha l\Delta}{2}\,(1 \pm J_3)\right]. \quad (11)$$

Therefore, the source term reduces to the difference of the backward intensities of crossed circular polarizations,

$$(I_+ - I_-) = |\varepsilon_b^+(z=l,t,\mathbf{r})|^2 - |\varepsilon_b^-(z=l,t,\mathbf{r})|^2, \quad (12)$$

which emphasizes the role of the feedback for the onset of the instability. Finally, using Eqs. (11) and (12), Eq. (5) becomes

$$\frac{\partial Q}{\partial \tau} = -[1 + (1+\Re)I_0]Q - \chi_0\{[\sin(\bar{\nabla}^2)\sin Q] \times [\cos(\bar{\nabla}^2)\cos Q] - [\cos(\bar{\nabla}^2)\sin Q][\sin(\bar{\nabla}^2)\cos Q]\}, \quad (13)$$

where Q is the nonlinear refractive index

$$Q = \frac{\Delta\alpha l}{2}\,J_3 \quad (14a)$$

and the operator $\Re$ is defined by the relation

$$\Re = R[\sin(\bar{\nabla}^2)\sin Q]^2 + [\cos(\bar{\nabla}^2)\cos Q]^2 + [\cos(\bar{\nabla}^2)\sin Q]^2 + [\sin(\bar{\nabla}^2)\cos Q]^2, \quad (14b)$$

with the definitions

$$\bar{\nabla}^2 = \frac{d\nabla_t^2}{k}, \quad I_0 = \varepsilon_0^2, \quad \chi_0 = R\Delta\alpha l I_0. \quad (15)$$

III. ANALYTICAL STUDY

The expansion of $\sin Q$ and $\cos Q$ in powers of Q on the right-hand side of Eq. (13) displays the nonlinearities involved near threshold. The stationary value of the order parameter Q_{st} is zero. Therefore, the quadratic nonlinearity occurring in the last term of Eq. (13) vanishes. In addition, the last term on the right-hand side of Eq. (16a) vanishes because of the relation $\cos(\bar{\nabla}^2)Q = \cos[(d/k)K^2]Q = 0$, for any critical wave number given by Eqs. (1). Finally, Eq. (13) becomes

$$\frac{\partial Q}{\partial \tau} = -\{1 + [1 + R(1 + Q^2 - \cos(\bar{\nabla}^2)Q^2)]I_0\}Q - \chi_0\left(\sin(\bar{\nabla}^2)Q - \frac{1}{3!}\sin(\bar{\nabla}^2)Q^3 - \frac{1}{2!}[\sin(\bar{\nabla}^2)Q] \times [\cos(\bar{\nabla}^2)Q^2]\right). \quad (16a)$$

The nonlinear terms are proportional either to RI_0 or to $\chi_0 = \Delta\alpha l R I_0$. In the limit of large $\Delta\alpha l$, the nonlinear terms proportional to RI_0 can be neglected with respect to those proportional to χ_0. Therefore, the model equation for the device with $\Delta\alpha l \gg 1$ becomes

$$\frac{\partial Q}{\partial \tau} = -\{1 + [1 + RI_0]\}Q - \chi_0\left[\sin(\bar{\nabla}^2)\left(Q - \frac{1}{3!}\,Q^3\right) - \frac{1}{2!}[\sin(\bar{\nabla}^2)Q)\right][\cos(\bar{\nabla}^2)Q^2]]. \quad (16b)$$

A. Linear analysis

Equation (16b) becomes, when keeping the terms proportional to Q,

$$\frac{\partial}{\partial \tau_0}\,Q = \mathscr{L}_0 Q, \quad (17)$$

with

$$\mathscr{L}_0 = -[1 + (1+R)I_0] - \chi_0 \sin \bar{\nabla}^2. \quad (18)$$

Equation (17) is solved by assuming a plane-wave input and by expanding Q in terms of Fourier modes

$$Q = \sum_{\kappa} q_\kappa e^{\lambda_\kappa t + i\boldsymbol{\kappa}\cdot\mathbf{r}} + \text{c.c.} \quad (19)$$

Therefore, when using the relation

$$\bar{\nabla}^{2n} e^{i\boldsymbol{\kappa}\cdot\mathbf{r}} = (-1)^n \bar{K}^{2n} e^{i\boldsymbol{\kappa}\cdot\mathbf{r}}, \quad (20)$$

with $\bar{K}^2 = dK^2/k$, Eqs. (17)–(20) give rise to the relation

$$\lambda_\kappa = -[1 + (1+R)I_0] + \chi_0 \sin \bar{K}^2, \quad (21)$$

leading to the marginal stability curve [16]

$$I_0 = [R\Delta\alpha l \sin(\bar{K}^2) - 1 - R]^{-1}. \quad (22)$$

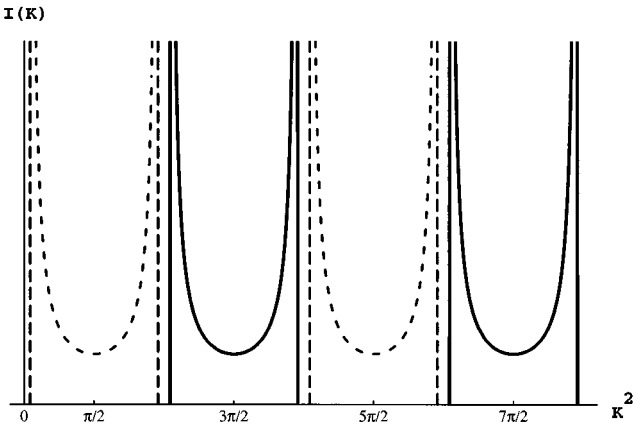

FIG. 1. Marginal stability curves for positive (full lines) and negative (dashed lines) detuning as a function of $\bar{K}^2$.

Eqs. (21) and (22) predict a static degenerate multiconical emission, which is displayed on Fig. 1. The critical wave numbers are given by Eqs. (1) and the threshold intensity is

$$I_{\mathrm{th}} \cong (R|\Delta|\alpha l)^{-1}. \tag{23}$$

B. Multiple scale analysis

With the scaling [20]

$$\begin{aligned} Q &= \varepsilon Q_1 + \varepsilon^3 Q_3 + \cdots , \\ I &= I_{\mathrm{th}} + \varepsilon^2 I_2 + \cdots , \\ \chi &= \chi_{\mathrm{th}} + \varepsilon^2 \chi_2 + \cdots , \\ \tau &= \tau_0 + \varepsilon^2 \tau_2 + \cdots , \\ \frac{\partial}{\partial \tau} &= \frac{\partial}{\partial \tau_0} + \varepsilon^2 \frac{\partial}{\partial \tau_2} + \cdots , \end{aligned} \tag{24}$$

we get, for terms proportional to ε, the linearized equation for Q_1 [see Eqs. (17)–(18)], while terms proportional to ε^3 give rise to

$$\begin{aligned} \frac{\partial}{\partial \tau_0} Q_3 - \mathscr{L}_{\mathrm{th}} Q_3 = &- \left(\frac{\partial}{\partial \tau_2} + (1+R) I_2 + \chi_2 \sin(\bar{\nabla}^2) \right) Q_1 \\ &+ \chi_{\mathrm{th}} \left(\frac{1}{3!} \sin(\bar{\nabla}^2) Q_1^3 + \frac{1}{2!} [\sin(\bar{\nabla}^2) Q_1] \right. \\ &\left. \times [\cos(\bar{\nabla}^2) Q_1^2] \right), \end{aligned} \tag{25}$$

where $\mathscr{L}_{\mathrm{th}}$ has the form defined in Eq. (18) for the threshold intensity I_{th}.

1. Amplitude equation

Let us assume an emission process involving at the first order a single critical wave number K_c, chosen among the infinite set (1), and expand Q_1 as

$$Q_1 = \tfrac{1}{2} \sum_{p=1}^{N} (a_p e^{i \mathbf{K}_p \cdot \mathbf{r}} + \mathrm{c.c.}), \tag{26}$$

where $|\mathbf{K}_p| = K_c$. The number N of wave vectors that determines the shape of the stable pattern expected above threshold will be deduced from the nonlinear analysis.

The right-hand side of Eq. (25) implies a solvability condition associated with expansion (26). (See Appendix A for details.) After collecting the terms of first and third order, we get the amplitude equation for any $A_p = \varepsilon \sqrt{|\chi_{\mathrm{th}}|/2} a_p$,

$$\frac{\partial}{\partial \tau} A_i = \mu A_i - A_i \left(|A_i|^2 + \sum_{j \neq i} \beta(\theta_{ij}) |A_j|^2 \right), \tag{27}$$

where θ_{ij} is the angle between $\mathbf{K}_i$ and $\mathbf{K}_j$ and $\mu = |\chi - \chi_{\mathrm{th}}|$. The Landau coefficient is given by the relation

$$\beta(\theta) = 1 - \cos[2\bar{K}_c^2 \cos(\theta)]. \tag{28}$$

The Landau coefficient obeys the relation $\beta(\theta) = \beta(\pi - \theta) = \beta(-\theta)$, because of the symmetry of the system, and is discontinuous [9] at $\theta = 0, \pi$ with $\beta(\theta \to 0) = \beta(\theta \to \pi) = 2\beta(0)$. In addition, it may display one or several minima in the interval $0 < \theta < \pi$, depending on $\bar{K}_c^2$. The number of minima of the Landau coefficient gives a first insight of the number of modes that may coexist. More precisely, knowledge of the magnitude of the $N \times N$ matrix elements $\beta(\theta_{ij})$ allows us to operate a primary selection of the pattern: Only if any $\beta(\theta_{ij}) \leqslant 1$ $(i,j = 1,N)$, may the N modes coexist [21].

In a general manner, the stationary weights $|A_j|^2$ are not equal. Nevertheless, for a regular pattern of $2N$-fold orientational order, each line of the matrix $\{\beta(\theta_{ij})\}$, with $\theta_{ij} = (\pi |i-j|)/N$, $|i-j| = 0, \ldots, N-1$, can be deduced from its neighbor by circular permutation, leading to equal amplitude fixed point solutions of the form $|A_l| = |A|$, with

$$|A|^2 = \mu \left[\sum_{m=0}^{N-1} \beta\left(\frac{m\pi}{N} \right) \right]^{-1}. \tag{29}$$

The stability of the $2N$ spot far-field pattern can be derived either from the stability analysis of the stationary solutions for the A_i or from the free-energy minimum. In the following sections, the two approaches will be considered for predicting the stable patterns associated with different critical wave numbers.

2. Free energy

In the neighborhood of a minimum of the marginality curve (Fig. 1), Eq. (16) is derivable from a potential

$$\frac{\partial Q}{\partial \tau} = - \frac{\delta G(Q)}{\delta Q}, \tag{30}$$

where the Lyapunov functional is

$$\begin{aligned} G(Q) = \int_{\mathscr{D}} \left(+ \frac{\eta - |\chi_{\mathrm{th}}|}{2} Q^2 + \frac{1}{4!} \left| \chi_{\mathrm{th}} \right| Q^4 \right. \\ \left. + \frac{1}{8} \left| \chi_{\mathrm{th}} \right| Q^2 \cos(\bar{\nabla}^2) Q^2 \right) d\mathbf{r}, \end{aligned} \tag{31}$$

with $\eta = [1 + (1+R) I_{\mathrm{th}}]$. (See Appendix B.) Therefore, the system will evolve to a stationary solution that minimizes the potential because of the inequality $dG/d\tau =$

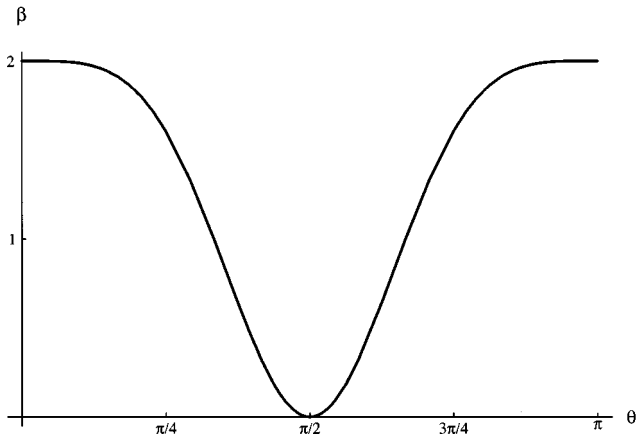

FIG. 2. Landau coefficient for $\bar{K}^2=\pi/2$ as a function of the angle θ between two wave vectors.

$-\int_{\mathscr{D}}(\partial Q/\partial\tau)^2 d\mathbf{r}\leqslant 0$. For the system under study, the potential $G(Q)$ is the free energy. When expanding the solution in Fourier modes, the free energy F can be written as

$$F=-\mu\sum_l |A_l|^2)+\tfrac{1}{2}\sum_l\sum_j \beta(\theta_{lj})|A_l|^2|A_j|^2, \quad (32)$$

with $(\partial/\partial\tau)A_i=-(\partial/\partial A_i^*)F$. The stationary free energy

$$F=-\frac{1}{2}\,\mu\sum_l |\bar{A}_l|^2 \quad (33)$$

becomes, for a regular pattern of $2N$-fold orientational order [9],

$$F=-\frac{1}{2}\,\mu^2 N\left[\sum_{m=0}^{N-1}\beta\left(\frac{m\pi}{N}\right)\right]^{-1}, \quad (34)$$

when using Eqs. (29) and (33). The minimum of the free energy deduced from Eq. (33) and/or Eq. (34) corresponds to the stable pattern of the system. It selects the number N and the shape of the pattern.

3. Application

The case (a),

$$\overline{K_c^2}=\frac{\pi}{2},$$

corresponds to an emission on the first cone for $\Delta>0$. The variation of the Landau coefficient $\beta(\theta)=1-\cos[\pi\cos(\theta)]$ is shown in Fig. 2 for $0\leqslant\theta\leqslant\pi$. It displays a single minimum equal to zero for $\theta=\pi/2$: Then two modes may coexist, for any $\beta(\theta)\leqslant 1$, with equal stationary amplitudes

$$|\bar{A}_1|^2=|\bar{A}_2|^2=\mu\,\frac{1}{1+\beta(\theta)}, \quad (35)$$

as solutions of Eq. (29), for $N=2$. The free energy (33) becomes, for two modes,

$$F=-\mu^2\,\frac{1}{1+\beta(\theta)}, \quad (36)$$

which displays its minimum for $\theta=\pi/2$. Therefore, the orthogonal structure minimizes the free energy, predicting the occurrence of square patterns.

Case (b),

$$\overline{K_c^2}=3\,\frac{\pi}{2}.$$

This case corresponds to an emission on the first cone for $\Delta<0$. The Landau coefficient

$$\beta(\theta)=1-\cos[3\pi\cos(\theta)] \quad (37)$$

displays three zeros, located at $\theta=\pm\arccos(\frac{2}{3})$ and $\pi/2$, as shown in Fig. 3(a). This behavior allows us to conjecture that four modes may coexist. The minima $\pm\arccos(\frac{2}{3})$, while near $\pi/4$ and $3\pi/4$, correspond to an irregular distribution of the spots on the critical circle of radius K_c, with unequal weights.

Let us study the the stability of the solution $\frac{1}{2}\Sigma_{p=1}^4 A_p(e^{i\mathbf{K}_p\cdot\mathbf{r}}+\text{c.c.})$, assuming *real* amplitudes A_p. The four Lyapunov exponents Eq. (36) generally depend on two angles $\theta=(\vec{K}_1,\vec{K}_2)$ and $\phi=(\vec{K}_1,\vec{K}_3)$, with $(\vec{K}_1,\vec{K}_4)=\pi-\theta$. For the sake of clarity we only show, on Fig. 3(b), the variation of the Lyapunov exponents as a function of θ, setting $\phi=\pi/2$: Among the four Lyapunov exponents, one of them is negative whatever θ might be and is not drawn; all the others are negative in a small domain around $\pi/4$ that does include $\arccos(\frac{2}{3})$. Therefore the stability analysis for the amplitude predicts stable patterns for any angle, between two adjacent modes, of magnitude of order $\pi/4$.

Nevertheless, the regular structure intuititively appears as the most probable. That conjecture is confirmed by the calculation of the free energy, Eqs. (33) and (34), that displays its absolute minimum for the eightfold orientational order pattern. See the variation of the free energy as a function of θ on Fig. 3(c).

Case (c),

$$\overline{K_c^2}=5\,\frac{\pi}{2}.$$

We assume that the system chooses the second critical wave number predicted by the linear stability analysis for an excitation on the focusing side $\Delta>0$. Then the Landau coefficient becomes

$$\beta(\theta)=1-\cos[5\pi\cos(\theta)], \quad (38)$$

which has five zeros $\arccos(\frac{4}{5})$, $\arccos(\frac{2}{5})$, $\pi/2$, $-\arccos(\frac{2}{5})$, and $-\arccos(\frac{4}{5})$. Let us assume that these angles are those of the mode 1 with the modes 2, 3, 4, 5, and 6, respectively. This geometry implies that other pairs of vectors make an angle very different from the above five angles, leading to a coupling coefficient larger than unity. For example, the angle $\theta_{2,6}$ between modes 2 and 6 is equal to $\pi-2\arccos(\frac{4}{5})$, leading to $\beta(\theta_{2,6})=1.25$, making unstable the irregular structure predicted by the zeros of the Landau coefficient (38).

The regular pattern might be stable because any $\beta(m\pi/6)$, $m=0,1,...,5$, is less than or equal to unity. Unfortunately, among the six Lyapunov exponents associated with the regular distribution, two of them are positive, which excludes the generation of a stable quasipattern of 12-fold orientational order.

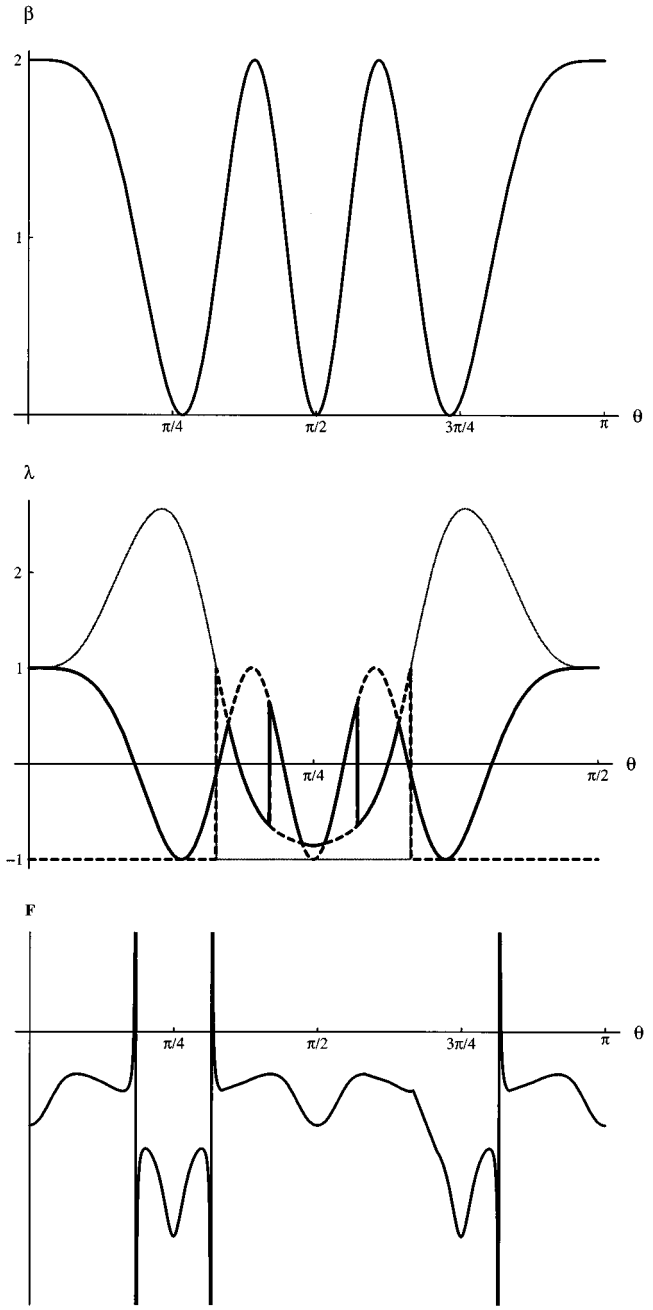

FIG. 3. $\bar{K}^2=3\pi/2$. (a) Landau coefficient as a function of the angle θ between two wave vectors. (b) Variation of the three Lyapunov exponents that are not always negative as a function of θ. (The other angle is fixed and taken to be equal to $\pi/2$.) (c) Variation of the free energy as a function of θ; a minimum occurs for $\theta=\pi/4$.

We may ask about the stable structure associated with the critical wave number $\bar{K}_c=\sqrt{5\pi/2}$. Actually, the stable structure corresponds to the minimum of the free energy. The stationary free energy for regular patterns, Eq. (34), is calculated as a function of N and is reported on Fig. 4, which displays the minimum for $N=2$. Therefore squares are also predicted to occur on the second cone associated with a focusing medium.

IV. NUMERICAL RESULTS

The amplitude of the electric field at the cell exit, which propagates in the forward direction with polarization orthogonal to the input beam polarization, is related to the order parameter Q

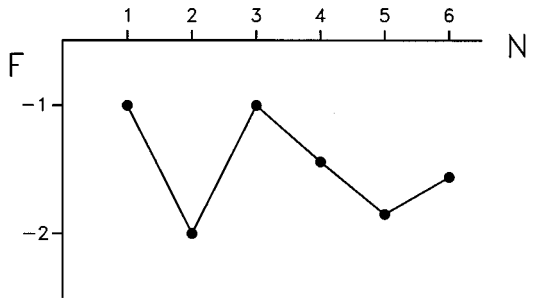

FIG. 4. Free energy for $2N$-fold orientational order pattern, as a function of N.

$$\varepsilon_{f,y}(l)=\varepsilon_x \sin Q$$

when using relation (10). Therefore, near threshold for Q small as compared with unity, we have approximately $\varepsilon_{f,y}(\mathbf{r},l)\propto Q$.

The numerical simulation integrates the equations of Ref. [16], deduced from Eqs. (5)–(7), by using a semi-implicit method and the free-space propagation in Eq. (9b) is treated by using the fast Fourier transform method. Different input shapes have been considered, either circular, square, or rhombic input.

Figure 5 displays the near and far-field intensities $|\varepsilon_{f,y}(\mathbf{r},l)|^2$ and $|\int d\mathbf{r}\, e^{-i\mathbf{K}\cdot\mathbf{r}}\varepsilon_{f,y}(\mathbf{r},l)|^2$ for the three cases discussed in Sec. III with the help of the model equation (16b). In Figs. 5(a) and 5(c) the detuning is positive and the input intensity close to the threshold value and the critical wave numbers $\bar{K}_c$ are $\sqrt{\pi/2}$ and $\sqrt{5\pi/2}$, respectively. The parameters are $\varepsilon_0=0.28$, $\Delta=200$, $\alpha l=0.07$, and $R=0.95$. The absorption is small and the product $\Delta\alpha l$ is equal to 14, so that the model equation (16b) should be valid. As predicted by the nonlinear analysis of Eq. (16b), the stable patterns are squares. The far-field orthogonal variables K_x and K_y of Figs. 5(a) and 5(c) are in arbitrary units, but it can be verified that the radii of the two circles on which the far-field spots are lying are in the ratio $\sqrt{5}$, in agreement with the linear stability analysis.

Figure 5(b) gives the numerical results for a negative detuning $\Delta=-200$ with the critical wave number $\sqrt{3\pi/2}$. As predicted analytically in Sec. III, a quasipattern of eightfold orientational order occurs. This structure is the result of nonlinearities and has been reproduced for different input windows. It can be verified that the eight spots of the far field are lying on a circle of radius equal to the predicted critical wave number and that the countour plot of the near-field displays a quasiperiodic pattern.

All these patterns are monoconical and stable not too far from threshold: For instance, for $\Delta=-200$, the eightfold orientational order pattern is stable for an input intensity increasing until 70% above threshold. When the intensity increases further, the system comes under the influence of the multiconical emission process [22]: Indeed, the regular eight spot pattern bifurcates to an irregular six spot pattern, next to a rectangle, and finally to sets of rectangles, designing a pic-

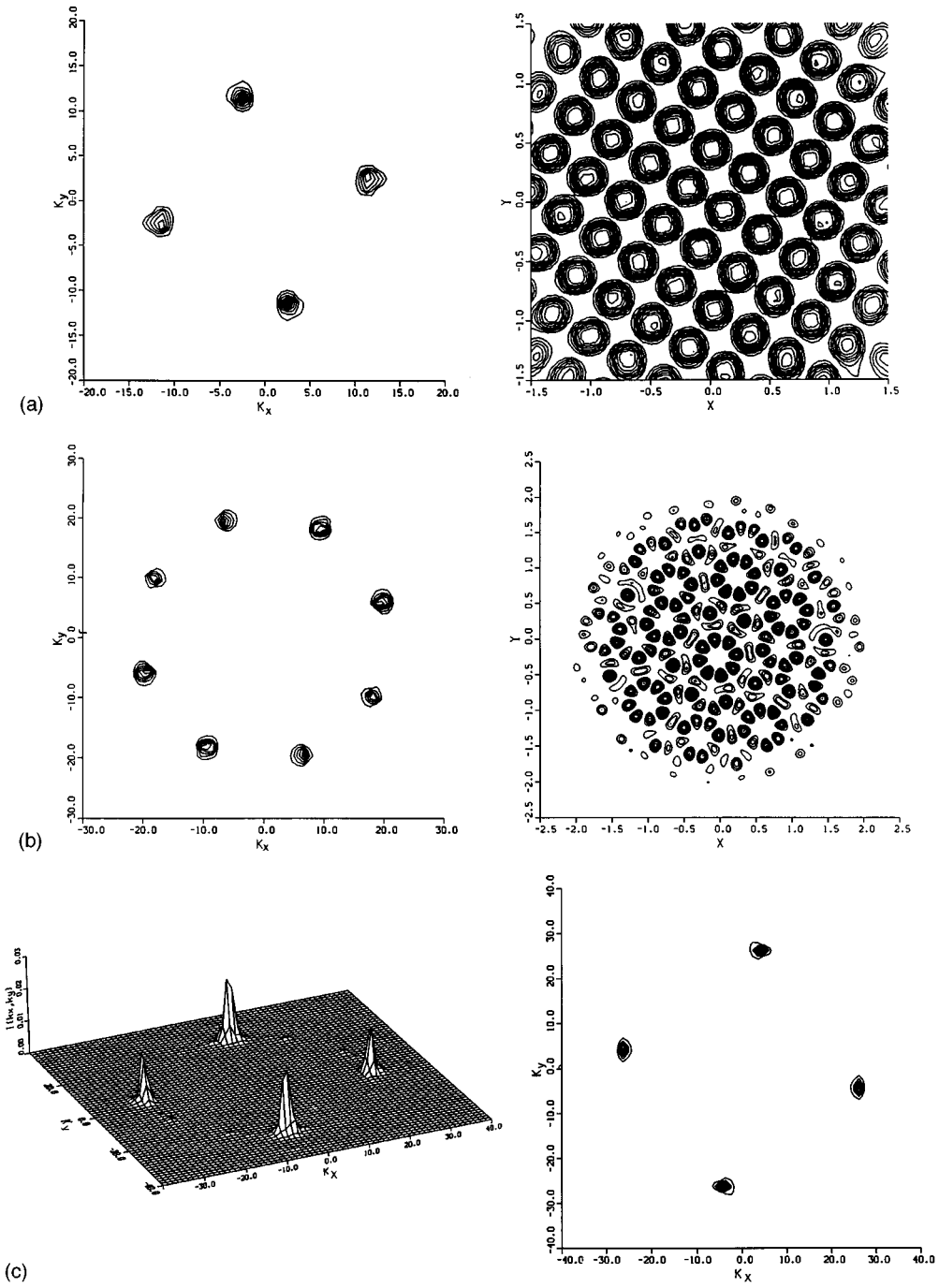

FIG. 5. Numerical results with the far field on the left-hand side and the near field on the right-hand side: (a) $\bar{K}_e^2=\pi/2$, (b) $\bar{K}_c^2=3(\pi/2)$, and (c) $K_c^2=5(\pi/2)$.

ture that can be geometrically understood with the help of the cubic nonlinearity, selecting the successive critical wave vectors.

V. CONCLUSION

It has been shown that a polarization instability provides a cubic nonlinearity, giving rise near threshold to a stable eightfold orientational order pattern. It appears to be the first prediction of quasipatterns spontaneously generated though nonlinearities in optics. The equations that have been numerically integrated are the model equations of the single-feedback-mirror device with rubidium atoms, which have quite well reproduced the flowerlike patterns observed in the limit of small aspect ratios[16]. Here the opposite limit of large aspect ratios has been considered, allowing us to assume a plane-wave input and consequently to perform a nonlinear analysis. The equations have be treated in the limit of large linear refractive index $|\Delta|\alpha l \gg 1$, which corresponds to the data of the device under study [11]. The role of this parameter on the onset of the instability is planned to be discussed elsewhere [22].

ACKNOWLEDGMENT

The numerical simulations have been performed with the IDRIS CNRS computer center support.

APPENDIX A

The component Q_3 can be expanded in Fourier modes such as Q_1. Therefore the resonant terms occur in the second member

$$-\left(\frac{\partial}{\partial t_2}+I_2+\chi_2\ \sin\ \bar{\nabla}^2\right)Q_1+\frac{1}{3!}\ \chi_{\rm th}\ \sin(\bar{\nabla}^2)Q_1^3 + \frac{1}{2!}\ [\sin(\bar{\nabla}^2)Q_1][\cos(\bar{\nabla}^2)Q_1^2]. \tag{A1}$$

Equation (25) should vanish. Setting $T=T_1+T_2+T_3$ with

$$T_1=-\left(\frac{\partial}{\partial t_2}+I_2+\chi_2\ \sin\ \bar{\nabla}^2\right)Q_1,$$

$$T_2=\frac{1}{3!}\ \chi_{\rm th}\ \sin(\bar{\nabla}^2)Q_1^3,$$

$$T_3=\frac{1}{2!}\ \chi_{\rm th}[\sin(\bar{\nabla}^2)Q_1][\cos(\bar{\nabla}^2)Q_1^2], \tag{A2}$$

by using the expansion (26) for $Q_1=\frac{1}{2}\Sigma_{p=1}^{N}(a_p e^{i\mathbf{K}_p\cdot\mathbf{r}}+\text{c.c.})$ and the same for the T_i, $i=1,2,3$,

$$T_i=\tfrac{1}{2}\sum_{p=1}^{N}\ [(T_i)_p e^{i\mathbf{K}_p\cdot\mathbf{r}}+\text{c.c.}], \tag{A3}$$

we obtain

$$(T_1)_p=-\left(\frac{\partial}{\partial t_2}+I_2-\chi_2\ \sin(\bar{K}^2)\right)a_p,$$

$$(T_2)_p=-\frac{1}{3!}\ \chi_{\rm th}\ \sin(\bar{K}^2)\tfrac{3}{4}\left(a_p|a_p|^2+2a_p\sum_{j\neq p}\ |a_j|^2\right),$$

$$(T_3)_p=-\frac{1}{2!}\ \chi_{\rm th}\ \sin(\bar{K}^2)\tfrac{1}{2}\Big([1+\tfrac{1}{2}\ \cos 4\bar{K}^2]a_p|a_p|^2 + \sum_{j\neq p}\ [\cos 4\ \bar{K}^2 + 2\ \cos(2\bar{K}^2)\cos(2\bar{K}^2\ \cos\ \theta_{p,j})]a_p|a_j|^2\Big). \tag{A4}$$

The products $\chi_2\sin(\bar{K}^2)$ and $\chi_{\rm th}\ \sin(\bar{K}^2)$ are positive whatever the sign of the detuning might be, as displayed either by Eqs. (1) and (15) or Eqs. (22) and (24). Then, the addition of the three resonant terms gives rise to the solvability condition

$$(T)_p=-\left(\frac{\partial}{\partial t_2}-I_2-|\chi_2|\right)a_p-\frac{1}{2}\ |\chi_{\rm th}|\Big(a_p|a_p|^2 + \sum_{j\neq p}\ [1-\cos(2\bar{K}^2\ \cos\theta_{p,j})]a_p|a_j|^2\Big)=0. \tag{A5}$$

Finally, collecting all the terms of the expansion (24) we obtain the amplitude equation (27) for an amplitude $A_p=\varepsilon\sqrt{|\chi_{\rm th}|/2}a_p$.

APPENDIX B

We look for a Lyapunov functional of the system and treat Eq. (16) near threshold in the case of an instability involving a single wave number K_c. Therefore we develop the operator $\bar{\nabla}^2$ around the eigenvalue $-\bar{K}_c^2$. It follows the relation

$$\sin\ \bar{\nabla}^2 Q=-\cos(\bar{\nabla}^2+\bar{K}_c^2)Q\cong-[1-\tfrac{1}{2}(\bar{\nabla}^2+\bar{K}_c^2)^2]Q\cong-Q. \tag{B1}$$

We can do the same expansion for $\sin\bar{\nabla}^2Q^3$ because the relevant vectors as a result of the combinations of three modes also have the length K_c. Therefore, we have

$$\sin\ \bar{\nabla}^2Q^3\cong-Q^3\ \sin(\bar{K}^2). \tag{B2}$$

It follows that Eq. (16) becomes

$$\frac{\partial Q}{\partial\tau}=-[1+(1+R)I_0]Q+|\chi_{\rm th}|\left[\left(Q-\frac{1}{3!}\ Q^3\right)-\frac{1}{2!}\ [Q\ \cos(\bar{\nabla}^2)Q^2]\right]. \tag{B3}$$

Therefore the Lyapunov functional

$$G(Q)=\int_D\Big(+\frac{\eta-|\chi_{\rm th}|}{2}\ Q^2+\frac{1}{4!}\ |\chi_{\rm th}|Q^4 + \frac{1}{8}\ |\chi_{\rm th}|Q^2\ \cos(\bar{\nabla}^2Q^2)d\mathbf{r}\Big) \tag{B4}$$

is easily shown to satisfy

$$\frac{\partial Q}{\partial\tau}=-\frac{\delta G(Q)}{\delta Q}, \tag{B5}$$

where

$$\delta G(Q)=G(Q+\delta Q)-G(Q). \tag{B6}$$

Indeed, the calculation of $\delta G(Q)$ gives, when using Eq. (B4),

$$\delta G(Q)=\int_D \delta Q\Big(+(\eta-|\chi_{\rm th}|)Q+\frac{1}{3!}\,|\chi_{\rm th}|Q^3 + \frac{1}{4}\,|\chi_{\rm th}|Q\,\cos(\bar{\nabla}^2)Q^2\Big)d\mathbf{r} + \int_D \frac{1}{4}\,|\chi_{\rm th}|Q^2\{\cos(\bar{\nabla}^2)Q\;\delta Q\}d\mathbf{r}. \quad \text{(B7)}$$

The last term that occurs in Eq. (B7) has been calculated by integrating by parts and taking account of the boundary conditions $(\partial^n/\partial x^n)_D=(\partial^n/\partial y^n)_D=0$. Then any term, such as

$$\int_{\mathscr{D}} Q^2\,\frac{\partial^{2n+m}}{\partial x^{2n}\partial y^{2m}}\,Q\;\delta Q\;d\mathbf{r},$$

related to the expansion of $\cos(\bar{\nabla}^2)$ is equal to

$$\int_{\mathscr{D}} Q\;\delta Q\,\frac{\partial^{2n}}{\partial x^{2n}}\,\frac{\partial^{2m}}{\partial y^{2m}}\,Q^2 d\mathbf{r},$$

so that the last two terms on the right-hand side of Eq. (B7) are equal. Therefore the relation (B5) is demonstrated and the function defined in Eq. (B4) is the Lyapunov functional of the system.

[1] M. C. Cross and P. C. Hohenberg, Rev. Mod. Phys. **65**, 851 (1993); A. C. Newell, T. Passot, and J. Lega, Annu. Rev. Fluid. Mech. **25**, 3995 (1993).

[2] J. Opt. Soc. Am. B **7** (6-7) (1990), special issue on transverse effects in nonlinear optical systems, edited by N. L. Abraham and W. J. Firth; SPIE Proc. **1840** (1991), special issue on transverse patterns in nonlinear optics, edited by N. N. Rosanov, A. A. Mak, and A. Z. Grasiuk; Chaos, Solitons Fractals **4** (1994), special issue on nonlinear optics structures, patterns, and chaos, edited by L. A. Lugiato and M. S. El Naschie.

[3] G. Grynberg, E. Le Bihan, P. Verkek, P. Simoneau, J. R. Leite, D. Bloch, S. Le Boiteux, and M. Ducloy, Opt. Commun. **67**, 363 (1988).

[4] A. Petrossian, M. Pinard, A. Maitre, J. Y. Courtois, and G. Grynberg, Europhys. Lett. **18**, 689 (1992).

[5] A. Maitre, thèse de doctorat, l'École Polytechnique 1994 (unpublished).

[6] Bo Christiansen, Preben Alstrom, and Mogens T. Levinsen, Phys. Rev. Lett. **68**, 2157 (1992).

[7] W. Stuart Edwards and Stéphane Fauve, C. R. Acad. Paris **315**, 417 (1992); Phys. Rev. E **47**, R788 (1993).

[8] A. A. Golovin, A. A. Nepomnyashchy, and L. M. Pismen, Physica D **81**, 117 (1995).

[9] Hanns Walter Müller, Phys. Rev. E **49**, 1273 (1994).

[10] G. Giusfredi, J. F. Valley, R. Pon, G. Khitrova, and H. M. Gibbs, J. Opt. Soc. Am. B **5**, 1181 (1988).

[11] G. Grynberg, A. Maitre, and A. Petrossian, Phys. Rev. Lett. **72**, 2379 (1994).

[12] A. S. Patrascu, C. Nath, M. Le Berre, E. Ressayre, and A. Tallet, Opt. Commun. **91**, 433 (1992).

[13] M. A. Vorontsov, N. G. Iroshnikov, and R. L. Abernathy, Chaos, Solitons Fractals **4**, 1701 (1994); E. Pampaloni, P. L. Ramazza, S. Residori, and F. T. Arecchi, Phys. Rev. Lett. **74**, 258 (1995).

[14] H. Adachihara and H. Faïd, J. Opt. Soc. Am. B **10**, 1242 (1993).

[15] S. Aumaitre, M. Le Berre, E. Ressayre, and A. Tallet, Quantum Semiclass. Opt. **7**, 795 (1995).

[16] M. Le Berre, D. Leduc, A. Maître, E. Ressayre, and A. Tallet, Opt. Commun. **118**, 447 (1995).

[17] M. W. Hamilton, R. J. Ballagh, and W. J. Sandle, Z. Phys. B **49**, 263 (1982).

[18] G. Grynberg, M. Vallet, and M. Pinard, Phys. Rev. Lett. **65**, 701 (1990).

[19] D. Suter, Opt. Commun. **86**, 381 (1991).

[20] P. Manneville, *Dissipative Structures and Weak Turbulence* (Academic, San Diego, 1990).

[21] See, for instance, S. Ciliberto, P. Coullet, J. Lega, E. Pampaloni, and C. Perez-Garcia, Phys. Rev. Lett. **65**, 2370 (1990). For an illustration, the free energy for a single mode, equal to $-\frac{1}{2}\mu^2$, from Eq. (33), becomes smaller than the free energy, for two modes, Eq. (36), when $\beta>1$.

[22] D. Leduc, M. Le Berre, E. Ressayre, and A. Tallet (unpublished).